

# 400 mW low noise continuous-wave single-frequency Er,Yb:YAl<sub>3</sub>(BO<sub>3</sub>)<sub>4</sub> laser at 1.55 μm

Yuanji Li,<sup>1</sup> Jinxia Feng,<sup>1</sup> Peng Li,<sup>1</sup> Kuanshou Zhang,<sup>1,\*</sup> Yujin Chen,<sup>2</sup> Yanfu Lin,<sup>2</sup>  
and Yidong Huang<sup>2</sup>

<sup>1</sup> State Key Laboratory of Quantum Optics and Quantum Optics Devices, Institute of Opto-Electronics, Shanxi University, Taiyuan 030006, China

<sup>2</sup> Key Laboratory of Optoelectronic Materials Chemistry and Physics, Fujian Institute of Research on the Structure of Matter, Chinese Academy of Sciences, Fuzhou, Fujian 350002, China

\*kuanshou@sxu.edu.cn

**Abstract:** We build up a LD end-pumped Er,Yb:YAB laser at 1.55 μm and improve the laser performance by end cooling the gain medium efficiently through a sapphire plate. 680 mW cw single transverse mode laser output was obtained with the slope efficiency of 16.3%. Using an etalon placed in the laser cavity, 400 mW cw single frequency 1.55 μm laser output was achieved with the slope efficiency of 11.8%. The laser power fluctuation was less than ± 1.3% in a given period of 1.5 hours. The 1.55 μm laser presents low noise properties, that the intensity and the phase noise reach the shot noise level for the analysis frequencies higher than 4 MHz and 5 MHz, respectively.

©2013 Optical Society of America

**OCIS codes:** (140.3480) Lasers, diode-pumped; (140.3570) Lasers, single-mode; (140.6810) Thermal effects.

## References and links

1. P. Laporta, S. Taccheo, S. Longhi, O. Svelto, and C. Svelto, "Erbium-ytterbium microlasers: optical properties and lasing characteristics," *Opt. Mater.* **11**(2-3), 269–288 (1999).
2. B. Denker, B. Galagan, I. Ivleva, V. Osiko, S. Sverchkov, I. Voronina, J. E. Hellstrom, G. Karlsson, and F. Laurell, "Luminescent and laser properties of Yb–Er:GdCa<sub>4</sub>O(BO<sub>3</sub>)<sub>3</sub>: a new crystal for eye-safe 1.5-μm lasers," *Appl. Phys. B* **79**(5), 577–581 (2004).
3. M. Brunel, A. Amon, and M. Vallet, "Dual-polarization microchip laser at 1.53 μm," *Opt. Lett.* **30**(18), 2418–2420 (2005).
4. J. H. Huang, Y. J. Chen, Y. F. Lin, X. H. Gong, Z. D. Luo, and Y. D. Huang, "High efficient 1.56 microm laser operation of Czochralski grown Er:Yb:Sr<sub>3</sub>Y<sub>2</sub>(BO<sub>3</sub>)<sub>4</sub> crystal," *Opt. Express* **16**(22), 17243–17248 (2008).
5. S. L. Braunstein and P. Loock, "Quantum information with continuous variables," *Rev. Mod. Phys.* **77**(2), 513–577 (2005).
6. J. X. Feng, X. T. Tian, Y. M. Li, and K. S. Zhang, "Generation of a squeezing vacuum at a telecommunication wavelength with periodically poled LiNbO<sub>3</sub>," *Appl. Phys. Lett.* **92**(22), 221102 (2008).
7. T. Eberle, S. Steinlechner, J. Bauchrowitz, V. Händchen, H. Vahlbruch, M. Mehmet, H. Müller-Ebhardt, and R. Schnabel, "Quantum enhancement of the zero-area Sagnac interferometer topology for gravitational wave detection," *Phys. Rev. Lett.* **104**(25), 251102 (2010), <http://prl.aps.org/pdf/PRL/v104/i25/e251102>.
8. T. Eberle, V. Handchen, J. Duhme, T. Franz, R. F. Werner, and R. Schnabel, "Strong Einstein-Podolsky-Rosen entanglement from a single squeezed light source," *Phys. Rev. A* **83**(5), 052329 (2011).
9. M. Mehmet, S. Ast, T. Eberle, S. Steinlechner, H. Vahlbruch, and R. Schnabel, "Squeezed light at 1550 nm with a quantum noise reduction of 12.3 dB," *Opt. Express* **19**(25), 25763–25772 (2011).
10. S. T. Lin, Y. Y. Lin, Y. C. Huang, A. C. Chiang, and J. T. Shy, "Observation of thermal-induced optical guiding and bistability in a mid-IR continuous-wave, singly resonant optical parametric oscillator," *Opt. Lett.* **33**(20), 2338–2340 (2008).
11. J. L. Liu, Q. Liu, H. Li, P. Li, and K. S. Zhang, "Low noise, continuous-wave single-frequency 1.5 μm laser generated by a singly resonant optical parametric oscillator," *Chin. Phys. B* **20**(11), 114215 (2011).
12. S. Taccheo, G. Sorbello, P. Laporta, G. Karlsson, and F. Laurell, "230-mW diode-pumped single-frequency Er:Yb laser at 1.5 μm," *IEEE Photon. Technol. Lett.* **13**(1), 19–21 (2001).
13. R. van Leeuwen, B. Xu, L. S. Watkins, Q. Wang, and C. Ghosh, "Low noise high power ultra-stable diode pumped Er-Yb phosphate glass laser," *Proc. SPIE* **6975**, 69750K, 69750K-9 (2008).
14. G. É. Pillet, L. I. Morvan, M. Brunel, F. Bretenaker, D. Dolfi, M. Vallet, J.-P. Huignard, and A. Le Floch, "Dual-frequency laser at 1.5 mm for optical distribution and generation of high-purity microwave signals," *J. Lightwave Technol.* **26**(15), 2764–2773 (2008).

15. N. A. Tolstik, S. V. Kurilchik, V. E. Kisel, N. V. Kuleshov, V. V. Maltsev, O. V. Pilipenko, E. V. Koporulina, and N. I. Leonyuk, "Efficient 1 W continuous-wave diode-pumped Er,Yb:YAl<sub>3</sub>(BO<sub>3</sub>)<sub>4</sub> laser," *Opt. Lett.* **32**(22), 3233–3235 (2007).
16. Y. J. Li, P. Li, J. X. Feng, and K. S. Zhang, "Theoretical and experimental investigation of Er<sup>3+</sup>,Yb<sup>3+</sup>:YAl<sub>3</sub>(BO<sub>3</sub>)<sub>4</sub> solid-state laser," *IEEE J. Quantum Electron.* submitted.
17. R. Weber, B. Neuenschwander, M. Mac Donald, M. B. Roos, and H. P. Weber, "Cooling schemes for longitudinally diode-pumped Nd:YAG rods," *IEEE J. Quantum Electron.* **34**(6), 1046–1053 (1998).
18. Y. J. Chen, Y. F. Lin, X. H. Gong, Q. G. Tan, Z. D. Luo, and Y. D. Huang, "2.0 W diode-pumped Er<sup>3+</sup>,Yb<sup>3+</sup>:YAl<sub>3</sub>(BO<sub>3</sub>)<sub>4</sub> laser at 1.5–1.6 μm," *Appl. Phys. Lett.* **89**(24), 241111 (2006).
19. M. Tsunekane, N. Taguchi, and H. Inaba, "Reduction of thermal effects in a diode-end-pumped, composite Nd:YAG rod with a sapphire end," *Appl. Opt.* **37**(15), 3290–3294 (1998).
20. F. Song, S. J. Liu, Z. H. Wu, H. Cai, X. Zhang, L. Teng, and J. G. Tian, "Determination of the thermal loading in laser-diode-pumped erbium-ytterbium-codoped phosphate glass microchip laser," *J. Opt. Soc. Am. B* **24**(9), 2327–2332 (2007).
21. R. Martínez Vázquez, R. Osellame, M. Marangoni, R. Ramponi, and E. Diéguez, "Er<sup>3+</sup> doped YAl<sub>3</sub>(BO<sub>3</sub>)<sub>4</sub> single crystals: determination of the refractive indices," *Opt. Mater.* **26**(3), 231–233 (2004).
22. D. Jaque, J. Capmany, J. Rams, and J. G. Sole, "Effect of pump heating on laser and spectroscopic properties of the Nd:YAl<sub>3</sub>(BO<sub>3</sub>)<sub>4</sub> self-frequency-doubling laser," *Appl. Phys. (Berl.)* **87**, 1042–1048 (2000).
23. S. Machida and Y. Yamamoto, "Quantum-limited operation of balanced mixer homodyne and heterodyne receivers," *IEEE J. Quantum Electron.* **22**(5), 617–624 (1986).
24. T. C. Zhang, J. P. Poizat, P. Grelu, J. F. Roch, P. Grangier, F. Marin, A. Bramati, V. Jost, M. D. Levenson, and E. Giacobino, "Quantum noise of free-running and externally-stabilized laser diodes," *Quantum Semiclass. Opt.* **7**(4), 601–613 (1995).

## 1. Introduction

Solid-state lasers at 1.5 μm have the advantages of compact structure, good beam quality, and excellent transparency in both atmosphere and fused-silica fiber, they are currently of great interest in the application fields, such as telecommunication, remote sensing, and laser range finder [1–4]. In particular, a low noise, continuous-wave (cw) single-frequency laser at 1.5 μm plays an important role in the scientific researches of quantum information and quantum optics [5–8]. More than 12 dB squeezed state at 1.5 μm have already been demonstrated based on a cw single-frequency erbium fiber laser [9]. However, since the fiber laser suffers large excess noise, narrow linewidth mode cleaners have to be used as a spatio-temporal filter in the experiments. Converting a cw single frequency Nd<sup>3+</sup> laser at 1.06 μm or 532 nm to 1.5 μm via optical parametric oscillation (OPO) is a practical way to obtain low noise 1.5 μm lasers [10, 11], but the system is relative complex and the nonlinear crystal should be temperature controlled accurately.

Fortunately, with Er<sup>3+</sup>,Yb<sup>3+</sup> codoped materials acting as gain mediums, laser diode (LD) pumped solid state lasers at 1.5 μm possess both a compact structure and low noise property. In 2001, S. Taccheo et al. demonstrated 230 mW cw single frequency Er<sup>3+</sup>,Yb<sup>3+</sup> co-doped phosphate glass laser at 1535.9 nm. Its relative intensity noise (RIN) presented a peak value lower than 92 dB/Hz and its level decreased below 160 dB/Hz for the frequencies higher than 8 MHz [12]. R. Leeuwen et al. obtained the low noise 1.5 μm laser by reduced the strong peak in the RIN spectrum at the relaxation oscillation frequency with a non-linear absorbing material inside the Er-Yb phosphate glass laser cavity [13]. G. Pillet et al. got 25 mW overall output power at 1.53 μm used a sapphire plate to cool an Er<sup>3+</sup>,Yb<sup>3+</sup> co-doped phosphate glass laser [14]. Recently, Er<sup>3+</sup>,Yb<sup>3+</sup> codoped YAl<sub>3</sub>(BO<sub>3</sub>)<sub>4</sub> (Er,Yb:YAB) crystal, which can emit 1.5 μm laser to 1 W level [15], has received great attention for its better characteristics. To give guidelines for laser design and improve the performance of Er,Yb:YAB lasers at 1.55 μm, we have established a theoretical model taking account of temperature-dependent thermal population distribution, temperature-dependent emission cross-section, and the thermal effects of gain medium [16]. From the theoretical predictions, the performance of cw Er,Yb:YAB lasers are expected to be optimized by lowering the laser crystal temperature.

In this paper, we build up a LD end-pumped Er,Yb:YAB laser at 1.55 μm and improve the laser performance by end cooling the gain medium efficiently using a sapphire plate. 680 mW cw single transverse mode (TEM<sub>00</sub>) laser and 400 mW cw single frequency laser with low noise properties at 1.55 μm are demonstrated.

## 2. Experiments and analysis

### 2.1 Experimental setup of the Er,Yb:YAB laser

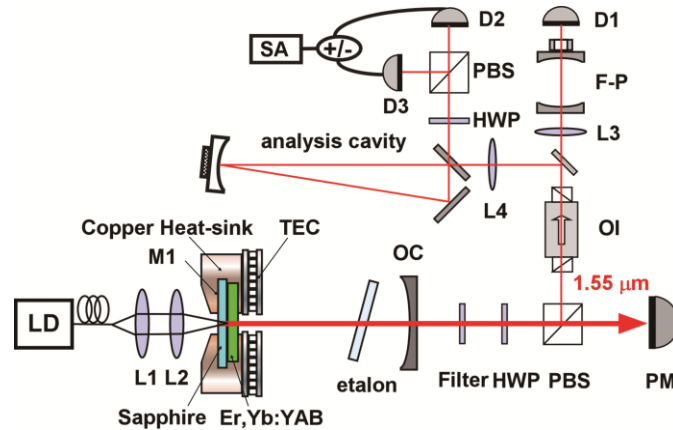


Fig. 1. Experimental setup of the Er,Yb:YAB laser. M1: input mirror; OC: output coupler; HWP: half wave plate; TEC: thermo-electric cooler; PBS: polarized beam splitter; PM: power meter; OI: optical isolator; F-P: Fabry-Perot interferometer; D1-D3: photodiode detectors; SA: spectrum analyzer.

The schematic of a LD end-pumped Er,Yb:YAB laser is shown in Fig. 1. Pump light is provided by a fiber-coupled LD with center wavelength of 976 nm and core diameter of 200  $\mu\text{m}$ , and is coupled into the laser crystal with a pump waist of 80  $\mu\text{m}$ . The resonator is a linear cavity formed by a plane input mirror (M1) and an output coupler (OC) with 100 mm radius of curvature. The input mirror with high-reflection coated at 1.55  $\mu\text{m}$  ( $R_{1.55 \mu\text{m}} > 99.5\%$ ) and high-transmission coated at 976 nm ( $T_{976 \text{ nm}} > 98\%$ ) is deposited onto the front face of a sapphire plate, whereas the rear face of the sapphire plate is uncoated and pressed into contact with an uncoated c-cut 0.74 mm-thick Er,Yb:YAB crystal doped with 25 at.%  $\text{Yb}^{3+}$  and 1.1 at.%  $\text{Er}^{3+}$ . It is worth noting that the sapphire and Er,Yb:YAB crystal have the similar refractive indexes at 1.55  $\mu\text{m}$  (1.746 and 1.7508, respectively), hence the interface reflectivity is approximately zero between the laser crystal and sapphire plate. The sapphire-Er,Yb:YAB composite-disk is mounted in a copper heat sink with a small hole in the center to allow the lasers to pass through. The radius of the small hole is 0.5 mm. The end cooled active-mirror configuration we designed is shown in Fig. 1. The copper heat sink is actively cooled at 15  $^{\circ}\text{C}$  via a thermo-electric cooler (TEC) and a temperature controller with an accuracy of  $\pm 0.01$   $^{\circ}\text{C}$  (YG-4S, YuGuang Co., Ltd). Owing to the sapphire is an excellent thermal conductor with the conductivity of 28 W/m·K, the Er,Yb:YAB crystal can be cooled efficiently. OC is a concave mirror partial-reflection coated at 1.55  $\mu\text{m}$  ( $R_{1.55 \mu\text{m}} \approx 98\%$ ) and placed 101 mm apart from the laser crystal.

For comparison, another cooling configuration is constructed without sapphire plate inside the copper heat sink. A plane input mirror with high-reflection coated at 1.55  $\mu\text{m}$  ( $R_{1.55 \mu\text{m}} > 99.5\%$ ) and high-transmission coated at 976 nm ( $T_{976 \text{ nm}} > 90\%$ ) is placed outside of the copper heat sink. The geometric length of the resonator is 105 mm to give a similar laser waist inside the gain medium.

### 2.2 Temperature distribution in Er,Yb:YAB crystal

To study how the performance of cw Er,Yb:YAB lasers can be optimized by lowering the temperature in the laser crystal, we should investigate firstly the temperature distributions in the Er,Yb:YAB crystal with and without sapphire cooling, respectively. If we assume the pump beam to be in a Gaussian field distribution, the heat source in the crystal induced by the absorption of the pump light can be read as [17]:

$$q(r, z) = \frac{2\alpha\zeta P_{in}}{\pi\omega_p^2(z)} e^{-2r^2/\omega_p^2(z)} e^{-\alpha z}, \quad (1)$$

where  $\alpha$  is the absorption coefficient of Er,Yb:YAB crystal,  $\zeta$  is the fractional thermal loading,  $P_{in}$  is the incident pump power,  $r$  and  $z$  are the transverse radial and longitudinal coordinates.  $\omega_p(z)$  is the pump spot radius and can be given by

$$\omega_p(z) = \omega_{p0} + \theta_p |z - z_0|, \quad (2)$$

where  $\omega_{p0}$  is the radius of pump waist, and  $\theta_p$  and  $z_0$  are the far-field half-angle and focal plane of the pump beam in the gain medium. In our calculations, the following parameter values are taken:  $\alpha = 43 \text{ cm}^{-1}$  [18],  $\zeta = 0.37$ ,  $P_{in} = 5 \text{ W}$ ,  $\omega_{p0} = 80 \text{ }\mu\text{m}$ ,  $\theta_p = 0.14\pi$ . The beam waist is located at one-third of the crystal ( $z_0 = 0.25 \text{ mm}$ ), which can be verified experimentally. Moreover, the thermal conductivities of sapphire plate and Er,Yb:YAB crystal were assumed to be independent on the temperature and coordinate, and the values are taken as  $28 \text{ W/m}\cdot\text{K}$  and  $4.7 \text{ W/m}\cdot\text{K}$ , respectively [18, 19].

The heat in the crystal will flow through the crystal surfaces in contacted with the copper heat sink, the air and the sapphire plate. We analyze the temperature distribution in the crystal using the finite-element-analysis method and the boundary conditions that the temperature is constant of  $15 \text{ }^\circ\text{C}$  on the crystal surfaces in contacted with the copper cooler, the heat transfer coefficient is  $50 \text{ W/m}^2\cdot\text{K}$  for crystal surfaces in contacted with air, and the heat transfer coefficient is  $1 \times 10^4 \text{ W/m}^2\cdot\text{K}$  for the contact surfaces between sapphire plate and Er,Yb:YAB crystal.

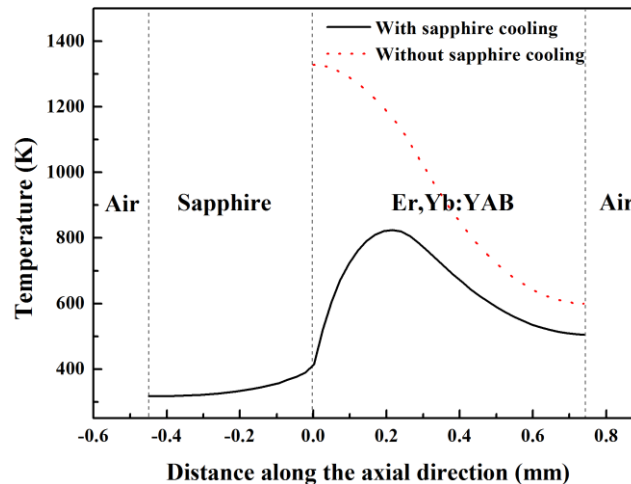


Fig. 2. Temperature distributions in the laser crystal under different cooling schemes.

The calculated temperature at the center of the pump region ( $r = 0$ ) in the Er,Yb:YAB crystal along the longitudinal axial direction is illustrated in Fig. 2. It can be seen that the maximum temperature in the Er,Yb:YAB crystal without sapphire cooling is about 1300 K and located at the entrance face of the crystal, while the maximum temperature in the crystal with sapphire cooling is significantly reduced to 800 K and its location is moved towards the center of the laser crystal. On the one hand, the great reduction of temperature in the Er,Yb:YAB crystal leads to a weaker thermal lens and benefits the  $1.55 \text{ }\mu\text{m}$  laser radiation that will be studied in the following experiments. On the other hand, owing to the location variation of the maximum temperature, the end effect of the crystal will be weakened and the thermal fracture limit will be scaled up.

### 2.3 Thermal lens effect in Er,Yb:YAB crystal

To determine the variation of the thermal focal length of the Er,Yb:YAB crystal experimentally, a knife method based on the characteristics of the TEM<sub>00</sub> laser output is used to measure the thermal focal length of the crystal [20].

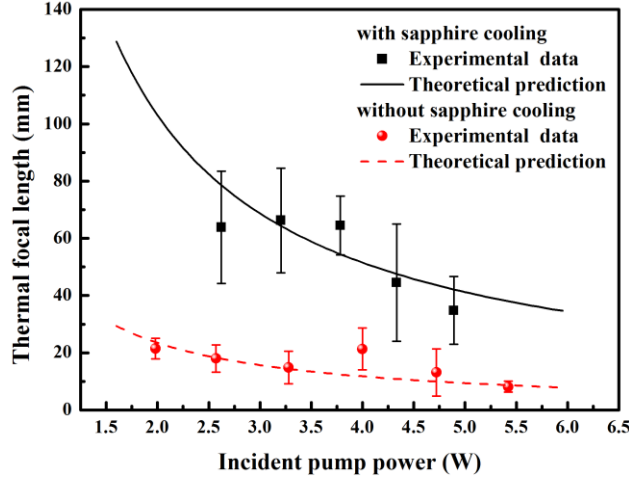


Fig. 3. Thermal focal length as a function of the incident pump power.

Figure 3 shows the measured and calculated thermal focal length of the Er,Yb:YAB crystal as a function of the incident pump power at two different cooling schemes. The solid circles and the solid squares give the experimental data without and with sapphire cooling, respectively. It can be seen that the thermal focal length of the Er,Yb:YAB crystal with sapphire cooling is about 34 mm at the incident pump power of 4.9 W, whereas the value of the crystal without sapphire cooling is only 13 mm at the pump power of 4.7 W. The error bars indicate the standard deviations for 5 times measurements.

The solid and dash curves are the calculated thermal focal length of the Er,Yb:YAB crystal using the model for end-pumped edge-cooled laser rod [20],

$$f_i = \frac{2\pi\kappa\omega_{pa}^2}{\xi P_{in}(1-e^{-\alpha l})} \cdot \frac{1}{\frac{dn_0}{dT} + (n_0 - 1)(1 + \nu)\alpha_T}, \quad (3)$$

where  $\omega_{pa}$  is the averaged pump waist in the laser crystal,  $n_0$  and  $dn_0/dT$  are the refractive index and the thermal-optic coefficient of laser crystal, respectively.  $\kappa$ ,  $\nu$ ,  $\alpha_T$  are the thermal conductivity, Poisson's ratio and thermal expansion coefficient, respectively. In the simulation, we took the parameter values of:  $\omega_{pa} = 120 \mu\text{m}$ ,  $n_0 = 1.7508$  [21],  $dn_0/dT = 11 \times 10^{-6} \text{K}^{-1}$ ,  $\nu = 0.28$ ,  $\alpha_T = 12 \times 10^{-6} \text{K}^{-1}$  [22],  $\alpha = 43 \text{cm}^{-1}$  [18], and  $P_{in} = 5 \text{W}$ . For the sapphire-cooling condition, the term of end-effect in the Eq. (3) was neglected and  $\xi = 0.22$  that is 0.6 times of the value for the non-sapphire-cooling condition. It can be seen that the measured data are in good agreement with the theoretical predictions.

## 2.4 1.55 $\mu\text{m}$ laser characteristics

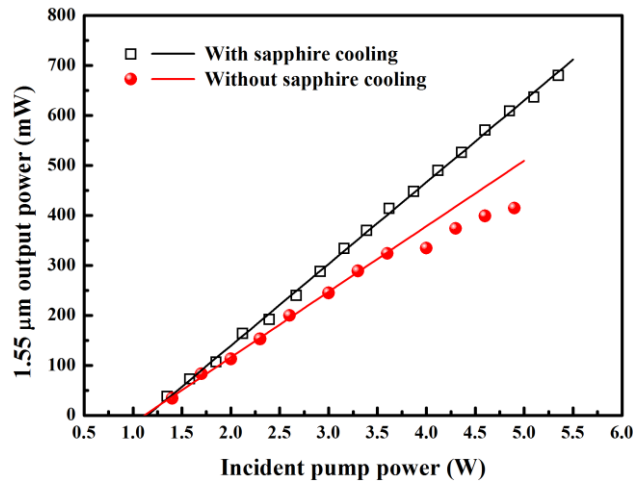


Fig. 4. Output power of cw TEM<sub>00</sub> 1.55  $\mu\text{m}$  laser as a function of the incident pump power for different cooling schemes.

Figure 4 shows the laser output versus the incident pump power for a cw Er,Yb:YAB laser at 1.55  $\mu\text{m}$ . The output power was measured by a power meter (*LabMax-TOP*, Coherent). The threshold power was about 1.1 W. A maximum cw 1.55  $\mu\text{m}$  laser output of 680 mW was obtained at the incident pump power of 5.35 W when the Er,Yb:YAB crystal was sapphire-cooled. The slope efficiency is 16.3%. As a comparison, when the Er,Yb:YAB crystal was non-sapphire-cooled, the maximum incident pump power of 4.9 W was employed considering the thermal fracture limit, and a maximum cw 1.55  $\mu\text{m}$  laser output of 420 mW was measured with a slope efficiency of 11.1%. The significant improvement of the laser slope efficiencies can be attributed to the lower temperature of crystal with sapphire cooling. Furthermore, we measured the laser beam qualities at the maximum laser outputs using a beam analyzer (Spricon M2-200-BB; CCD: SP-1550M). That are  $M^2_x = M^2_y = 1.18$  for the non-sapphire-cooled laser and  $M^2_x = M^2_y = 1.1$  for the sapphire-cooled laser. The measured results indicate that the lasers are TEM<sub>00</sub> operation.

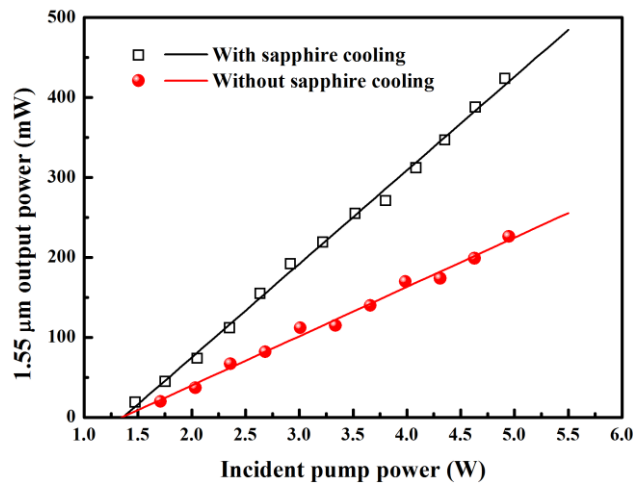


Fig. 5. Output power of cw single frequency 1.55  $\mu\text{m}$  laser as a function of the incident pump power for different cooling schemes.

To get a cw Er,Yb:YAB laser at 1.55  $\mu\text{m}$  with single frequency operation, we inserted a 0.3 mm-thick uncoated fused silica as an etalon in the laser cavity. The etalon was placed in a copper oven and temperature controlled at 30  $^{\circ}\text{C}$  by homemade temperature controller. Figure 5 shows the cw 1.55  $\mu\text{m}$  laser outputs versus the incident pump power. At maximum incident pump power of 4.9 W, maximum cw 1.55  $\mu\text{m}$  laser outputs of 400 mW and 230 mW were obtained with slope efficiencies of 11.8% and 6.2% when the Er,Yb:YAB crystal was sapphire-cooled and non-sapphire-cooled, respectively. The longitudinal mode of the cw Er,Yb:YAB laser was monitored using a homemade scanning Fabry-Perot (F-P) interferometer (Free Spectral Range: 750 MHz, Fineness: 720) and recorded by a digital telescope (Tektronix DPO4054). The transmitted intensity from F-P interferometer is shown in Fig. 6 that indicated the laser was single frequency operation.

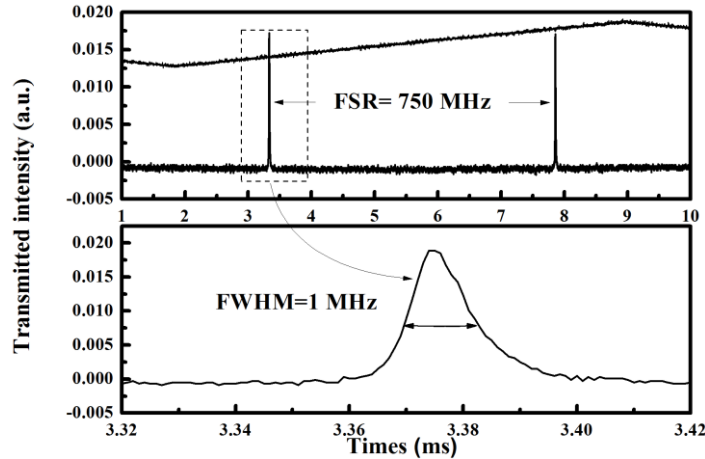


Fig. 6. Transmitted intensity from F-P interferometer.

The long term power stability of the cw single frequency Er,Yb:YAB laser was measured by the power meter (*LabMax-TOP*, Coherent), as shown in Fig. 7. The measured power fluctuation was less than  $\pm 1.3\%$  in a given period of 1.5 hours.

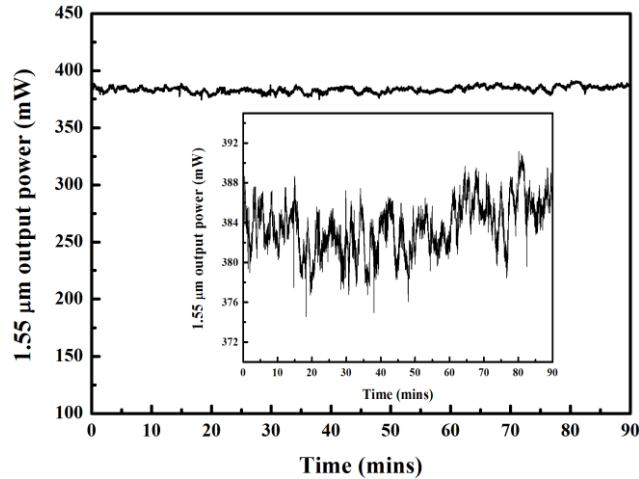


Fig. 7. Power fluctuation of the cw single-frequency 1.55  $\mu\text{m}$  laser.

It is worthy to investigate the noise characteristics of a cw single-frequency Er,Yb:YAB laser. The intensity noise of the 1.55  $\mu\text{m}$  laser was measured using a balanced homodyne detection system [23], that formed by HWP, PBS and a pair of low noise, broadband detectors

(D2 and D3), as shown in Fig. 1. The common-mode rejection ratio of the D2 and D3 is more than 40 dB. The sum and difference of the detected signals were recorded by a spectrum analyzer (N9010A, Agilent). The sum signal gives the intensity noise power of the 1.55  $\mu\text{m}$  laser and the difference signal gives the shot noise limit (SNL), which was calibrated by a thermal white light source. To investigate the detail of the intensity noise at the range of low frequency, especially around the resonant relaxation oscillation (RRO) frequency, the parameters of the spectrum analyzer was set as resolution bandwidth of 1 kHz, video bandwidth of 100 Hz, and sweep time of 1 s. For performing the noise spectrum measurement, the laser power injected into the D2 and D3 was precisely adjusted to 4 mW. The electronic noise level of the detectors is 20 dB below the SNL. The noise spectra of the 1.55  $\mu\text{m}$  laser are plotted relative to the SNL on a log-log scale and 0 dB indicates that the noise level equals to the SNL, as shown in Fig. 8. It can be seen, although the intensity noise presented a peak value of 47 dB above SNL at the RRO frequency of 200 kHz, the intensity noise reached the SNL for frequencies above 4 MHz. To investigate the phase noise of 1.55  $\mu\text{m}$  laser, an empty off-resonance ring cavity (the analysis cavity in Fig. 1) was used as a phase-to-amplitude converter [24]. The analysis cavity has a finesse of 220 and bandwidth of 1.4 MHz, allowing for a complete conversion of phase to intensity noise for analysis frequencies higher than 1.5 MHz. The phase noise of the 1.55  $\mu\text{m}$  laser was measured at each analysis frequency by scanning the cavity with triangular wave of 2 Hz. As shown in Fig. 8, the squares are the measured phase noise power relative to the SNL. It can be seen that phase noise of the 1.55  $\mu\text{m}$  laser reaches the SNL for the analysis frequencies higher than 5 MHz.

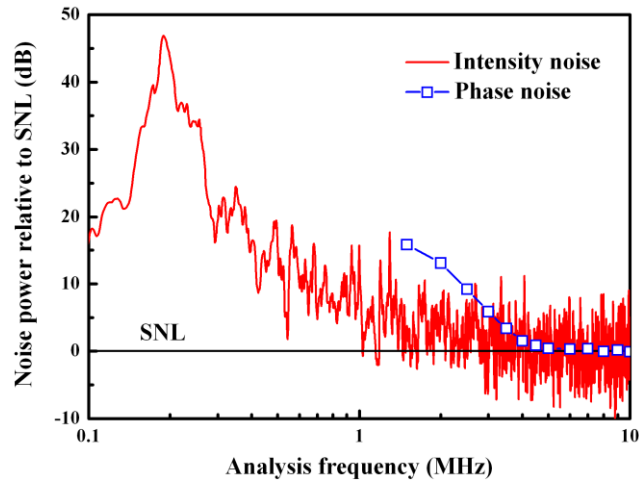


Fig. 8. Measured intensity and phase noise power of the cw single frequency Er,Yb:YAB laser at 1.55  $\mu\text{m}$  as the function of the analysis frequency. The parameters of the spectrum analyzer: resolution bandwidth is 1 kHz, video bandwidth is 100 Hz, and sweep time is 1 s.

### 3. Conclusion

Based on the investigation of the temperature distribution and the thermal lens effect in the laser crystal, we built up a LD end-pumped Er,Yb:YAB laser at 1.55  $\mu\text{m}$  and improved the laser performance by end cooling the gain medium efficiently through a sapphire plate. A maximum cw TEM<sub>00</sub> 1.55  $\mu\text{m}$  laser output of 680 mW was obtained with the slope efficiency of 16.3%. Using an etalon placed in the laser cavity, a cw single frequency 1.55  $\mu\text{m}$  laser was demonstrated. A maximum cw single frequency 1.55  $\mu\text{m}$  laser output of 400 mW was achieved with the slope efficiency of 11.8%. The measured power fluctuation was less than  $\pm 1.3\%$  in a given period of 1.5 hours. The noise characteristics of the laser were also investigated; the intensity and the phase noise reach the SNL for the analysis frequencies higher than 4 MHz and 5 MHz, respectively. This kind of low noise cw single frequency

lasers at 1.55  $\mu\text{m}$  can be used in the application fields such as laser remote sensing, high-precision measurement, and quantum information.

### **Acknowledgments**

This work was supported in part by the National Natural Science Foundation of China (61227015), the National Program for Basic Research in China (2010CB923101) and National Major Scientific Equipment Developed Project of China (2011YQ030127).